The role of repulsive and attractive forces in low-energy (3–15 eV) electron stimulated desorption of anions from molecular layers grown on clean and contaminated metallic substrates

Norhan Omar, Pierre Cloutier, Christophe Ramseyer, Léon Sanche, Michel Fromm

The role of repulsive and attractive forces in low-energy (3-15 eV) electron stimulated desorption of anions from molecular layers grown on clean and contaminated metallic substrates

Norhan OMAR[a], Pierre CLOUTIER[b], Christophe RAMSEYER[a], Léon SANCHE[b], Michel FROMM[a,*]

[a]*Laboratoire Chrono-Environnement, ULR CNRS 6249, Université de Franche-Comté, 25030 Besançon cedex, France.*
[b]*Department of Nuclear Medicine and Radiobiology, Université de Sherbrooke, Sherbrooke, Canada.*

Abstract

CD_4 is cryocondensed on three substrates : oxized tantalum, gold and platinum, with thicknesses from 1 to 12 monolayers (ML). For a low surface charge ratio, the total potential is repulsive starting from the third layer. Experimentally, when few ML of CD_4 are deposited on Pt cleaned by heating, dissociative electron attachment (DEA) is strongly inhibited, contrary to Ta or Au which are contaminated substrates. As the thickness increases, we observe that resonance peaks broaden and their maximum moves to higher electron energies. Both peak area and maximum anion yields tend to a plateau. Total collision cross-sections for both desorbed ions and incident electrons allow the observed peak behaviors to be explained. Adsorption energies show that when both condense on Pt or Ta, CD_4 and residual water exclude each other. Inhibition of DEA for small CD_4 thicknesses on Pt and the reason why water contaminated substrates provide significant desorption yields are explained.

Keywords: Low energy electrons, dissociative electron attachment, CD_4, clean Pt, contaminated substrates, anionic desorption

*Corresponding author
Email address: michel.fromm@univ-fcomte.fr (Michel FROMM)

1. Introduction

1.1. General considerations

Low energy electrons (LEEs) incident on molecules physiosorbed on a conductive substrate induce electronic excitation and the formation of transient negative ions (TNIs). These phenomena can result in the desorption of ions, ground state neutrals, or electronically and vibrationally excited atoms, radicals and molecules. Seminal Electron Stimulated Desorption (ESD) studies addressed the case of small molecular adsorbates on clean metal surfaces under ultrahigh vacuum conditions [1]. Up to the late 1970's, most of these studies focused on positive ion desorption [2], because of their ease of detection. In the early 1980s, ESD of anions of a few electron volts (eVs) from physisorbed molecules was observed, well below the threshold for dipolar dissociation (DD). Such anions were created via the dissociative electron attachment (DEA), mechanism [3], i.e., from the dissociation of a TNI into a radical and a stable anion fragment. The scope of applications of anion ESD has expanded over numerous fields of research, such as the fundamental radiation chemistry of deoxyribonucleic acid (DNA) exposed to secondary LEEs [4, 5, 6, 7, 8], and more generally, LEE-induced chemistry of various condensed-phase dissociative processes [9, 10], including reactions for molecules in ice mantles coating interstellar dust grains [11, 12, 13]. As the chemistry of LEEs emerged, it became increasingly recognized that such electrons could efficiently trigger specific reactions and that several factors at and near the surface of solids could modify the yields of ESD of anions.

Incident electrons in multilayer molecular films and within a conductive substrate lose energy and modify their initial angular distributions. Thus, electron energy losses necessarily affect the energy of TNIs and that of DEA yields, which occur at specific energies. Furthermore, electrons penetrating the film and other charged species formed during sample irradiation can induce surface potentials, which can also shift the energies of TNIs and DEA peaks in the electron-energy dependence of the ESD yields. Energy thresholds for these processes and DD can also be affected, as well as the kinetic energy distribution of the desorption fragments. Ions formed at the film-vacuum interface or within multilayer films of condensed molecules can be trapped inside deep

attractive potential wells created by induced charge polarization, resulting in an additional barrier to desorption [14]. The anions created by electron impact can also collide with the unperturbed adsorbed species, which can reduce their kinetic energy, and thus hinder their desorption. Furthermore, reactive scattering can also modify the nature and quantities of the desorbing anions [15]. In anion ESD, post-dissociation image-charge effects are considered to arise from the pull on the anion by the polarization forces, as shown by ESD measurements of O_2 molecules condensed on a spacer dielectric layer of argon pre-deposited on a metal substrate. From such an experiment, it was deduced that screening of the metal image force by the Ar atoms increased the number of desorbing O^- ions via DEA, for several reasons, including the reduction of O^- ions drawn back to the metal by the charge-induced polarization force [14].

Although these perturbations can modulate considerably anion ESD yields and their angular distributions, presently, there is no detailed kinetic studies coordinated with experimental data. Furthermore, we have little information of the effects of substrate surface contaminants on ESD yields. With relatively simple molecules that can be evaporated in vacuum, it has been possible to deposit them onto fairly clean substrates and maintain well-defined experimental conditions. This is far from being the case with non-evaporable biomolecules that have been increasingly investigated by ESD in ultra-high vacuum since the discovery of DEA to DNA [16]. In these ESD experiments, the molecules are usually deposited by lyophilization or spin coating on gold or tantalum substrates. Although such manipulations are often performed under controlled conditions [17, 18], the substrates have been previously exposed to the atmosphere.

In this work, we address the problem of attractive and repulsive forces created in thin molecular films during ESD experiments. The forces and the corresponding potentials are calculated from a lattice representation of the charges involved. The theoretical results are compared to those of ESD experiments obtained from 3-15 eV electrons impinging on films of deuterated methane (CD_4). Different experiments are performed with CD_4 molecules deposited on a clean platinum (Pt) surface and contaminated tantalum (Ta) and on gold (Au) substrates. The latter two substrates were often utilized in LEE-biomolecules investigations and represent two different types of surface modification due to exposure to the atmosphere. Ta oxidizes in contact with oxygen in

the atmosphere, whereas Au is relatively inert and thus its surface is expected to be composed of adsorbed impurities.

1.2. ESD via dissociative electron attachment

In this section, we first describe the energetics involved in DEA to an isolated diatomic molecule AB made of atom A and B, i.e.,

$$AB + e^- \rightarrow AB^{-*} \rightarrow A^* + B^- \tag{1}$$

where AB^{-*} is the TNI.

The excess reaction energy can be written as [19]:

$$E = E_i - (D_0 + E^* - E_a) \tag{2}$$

where D_0 is the dissociation energy of the neutral molecule, i.e., the A-B bond energy of the neutral parent molecule AB. E_a is the electron affinity of atom B, E_i the incident electron energy, and E^* the excitation energy of the neutral fragment. The excess energy in Eq. 2 is shared between the dissociating fragments as kinetic energy. From energy and momentum conservation, the kinetic energy of the B^- anion is given in Ref. [19] by:

$$T_{B^-} = (1-\beta)[E_i - (D_0 + E^* - E_a)] \tag{3}$$

where β is the ratio of the specific anion fragment mass to the mass of the parent molecule ($\beta = \frac{m_B}{m_{AB}}$). This relation is particularly true for the ideal case of a low-pressure gas-phase experiment, where no perturbation arises from a substrate or a deposited sample layer. For a condensed phase sample, additional interactions described in Section 1.1 come into play and the isolated electron-molecule Eq. 3 is no longer valid. A modified expression which includes additional perturbations due to the condensed phase and a metallic substrate has already been proposed [20] as

$$T_{B^-} = (1-\beta)[E_i - \Delta E_i - D_0 - E^* + E_a] - \beta E_{pol} - \Delta E_{B^-} \tag{4}$$

ΔE_i is the amount of electron energy loss prior to DEA. The electrostatic E_{pol} term represents the charge-induced average polarization barrier, which must be overcome by the anion fragment during desorption, including the charge-image potential. This term is certainly valid in case of physisorbed anions, but is obviously not suitable for chemisorbed species, where large charge transfer can occur between the metallic surface and the adsorbed anion. Chemisorption is therefore not considered in our analyses. ΔE_{B^-} is the kinetic energy lost by the B^- fragment due to inelastic collisions with adjacent molecules (B^-, A^*, AB^{-*} and AB) in the solid or near the surface prior to desorption. The potential interactions between B^- and the other fragments (B^-, A^*, AB^{-*} and AB) in the adsorbed layer are not explicitly included in this expression. Repulsive interactions may, however, counterbalance the attractive potential induced by the negatively charged departing fragment. Thus, they can help to overcome the charge-induced polarization barrier of the substrate, increase the kinetic energy perpendicular to the surface, and hence influence the measured desorption yields. These repulsive interactions depend on the number of negative charges in the adsorbed film and on the distribution of the charges in this film, e.g., isolated vs aggregates. The terms -βE_{pol} and -ΔE_{B^-} in Eq. 4 have been replaced with the 3 terms $E_{B^-/S}$, $E_{B^-/Q}$ and E_{B^-/Q^-} that have been calculated in our study. The polarization energy is now detailed through the terms $E_{B^-/S}$ (image charge and adsorption energy, the latter was not considered in the present study) and through the term $E_{B^-/Q}$ (polarization inside the film, interactions with the neutral fragments; Q=AB, A). The last term, E_{B^-/Q^-} stands for repulsive interactions between negative charges in the film. These two antagonistic electrostatic terms can be readily implemented in the following equation:

$$T_{B^-} = (1-\beta)[E_i - \Delta E_i - D_0 - E^* + E_a] + [E_{B^-/S} + E_{B^-/Q} + E_{B^-/Q^-}]. \quad (5)$$

This formulation is expected to be valid when multilayer films are sufficiently thick to minimize the effects of the substrate on the intrinsic properties of TNIs [21], such as lifetime and number of decay channels.

In addition to model calculations, we have conducted experiments to highlight the

different aspects mentioned in this subsection. It addresses more specifically the effect of repulsive electrostatic interaction energies due to the presence of negatives charges in molecular layers. Results of anion ESD experiments are presented for different substrates mentioned in Section 1.1 covered with different thicknesses of deuterated methane, forming single and multilayer films. We emphasize the contribution of contaminants present on substrates, namely when the substrate is not cleaned by heating it in vacuum. The chosen model film composed of CD_4 molecules avoids misinterpretations in the mass analyses of the ESD anions arising from any contaminant producing atomic hydrogen. H^- anions can indeed copiously desorbed from common impurities in vacuum that can condensed on films, such as water and hydrocarbons, whose contributions are not estimated in our calculations. The attractive part of the potential induced in the metallic substrates is calculated using the image-charge approach with the metal treated as a continuum. The repulsive interactions between the B^- ions are evaluated as the average of coulombic interactions for an inhomogeneous distribution of anions inside a CD_4 layer of various thicknesses. Surface impurities arise from both atmospheric pollutants and molecules presents in vacuum. Due to substrate adsorption kinetics, the distribution of surface contaminants is expected to be different in ultra-high vacuum compared to that under atmospheric conditions.

2. Materials and methods

2.1. ESD experiments

A complete description of the ESD setup is given elsewhere [22, 23]. Briefly, ESD experiments were performed using a TOF mass spectrometer (Kore-5000 Reflectron TOF analyzer) in a UHV system (base pressure of 3×10^{-10} Torr). The sample was bombarded by a pulsed LEE beam from a Kimball Physics ELG-2 gun incident at an angle of 40° with respect to the sample surface normal. The cross-sectional area of the beam is estimated to be about 2 mm^2. The time averaged incident current was $\sim$ 5.0 nA, delivered in pulses of 800 ns duration at 5 kHz. A negative potential pulse (-2.4 kV with a pulse width of 2 ms) was applied to the sample immediately following each electron pulse to inject anions from the sample region into the entrance optics of

the TOF mass analyzer that was positioned along the sample surface normal. Anion desorption yields measured as a function of electron energy are termed yield functions; they were measured from 3 to 15 eV (which are nominal energy values prior to energy calibration) with electron energy increments of 0.25 eV and 50 000 electron pulses per point. Sample CD_4 films were condensed onto three different types of metal substrates : a clean polycrystalline Pt foil (Goodfellow), and tantalum and gold substrates, both prepared by evaporation of the metal onto a silicon wafer, evaporated Au and Ta are amorphous layers. The Pt foil can be cleaned by heating immediately prior to CD_4 condensation, but the other substrates, which are introduced into UHV system via a load-lock, cannot be resistively heated before sample condensation. Substrates are cooled at $\sim$ 15 K with a closed-cycle He compressor (APD Cryogenics).

The CD_4 vapor (Sigma-Aldrich, purity > 99.99 %, degassed by freeze thaw cycles under vacuum) was introduced from a small turbopump, manifold volume at room temperature, into the UHV system via an all-metal valve and a stainless-steel capillary tube that terminate $\sim$ 1 cm from the metal substrate and at an angle of 45° to the surface normal. The quantity of the deposited gas was evaluated by the differential drop of pressure in the manifold, measured by a capacitance manometer. The quantity of CD_4 gas deposited on the substrates is expressed in monolayers (ML), where 1 ML is that quantity required (within a precision of $\pm$ 30 %) to form a molecular monolayer, as determined by a volumetric dosing procedure [24] and film density calculations.

2.2. Potential energy curve calculations

To mimic the charging of a CD_4 multilayer film upon electron trapping and DEA, we generated an inhomogeneous distribution of discrete charged sites N_c inside a CD_4 sample. Those later are considered as a uniform unstructured metal surface represented by a continuum, i.e. described only by its relative permittivity (see Eqs. 6 and 7).

CD_4 layers were considered to form an incommensurable hexagonal lattice on the investigated substrates. The equilibrium distances between the adsorbed layer and substrate and the lattice parameter of the adsorbate were determined by optimizing the electronic energy of the adsorbate/substrate systems with the Vienna Ab initio Simulation Package, VASP [25, 26, 27, 28, 29]. We obtained a lattice parameter of 3.91 Å for

CD_4 layers. For a modeled area of 100 × 100 Å^2, this leads to 100/4 × 100/4 = 625 CD_4 molecules per monolayer. The equilibrium distances were found to be D = 3.2, 2.8 and 2.9 Å for platinum, tantalum and gold respectively.

The repulsive interaction potential between the departing anion B^- of charge Q_i and the other negative charges Q_j embedded in the CD_4 layers of dielectric constant ε_2 can be written as:

$$V_{(r)} = \sum_{i=1,j\neq i}^{N_c,N_c} \frac{1}{4\pi\varepsilon_0\varepsilon_2} \frac{Q_i Q_j}{r_{ij}} \tag{6}$$

Where r_{ij} is the distance between Q_i and Q_j charges. Here, Q_j can represent not only charges from TNIs, stable anions resulting from DEA and trapped electrons, but also those resulting from image charges in the metallic substrate.

In the charge-image approach, the attractive potential experienced by an anion of charge Q formed within a CD_4 layer (ε_2=1.1) [30] and located at a distance D from the surface of a substrate of permittivity ε_3 can be expressed as :

$$V_{(D)} = \frac{1}{4\pi\varepsilon_0\varepsilon_2} \frac{\varepsilon_3 - \varepsilon_2}{\varepsilon_3 + \varepsilon_2} \frac{-Q^2}{2(2D)} \tag{7}$$

with ε_3= 6.9 and 25.0 for gold and tantalum oxide respectively [31, 32]. For the gold surface, due to its chemical inertness in air, we used the relative permitivity of pure gold. On the contrary, as the tantalum surface is oxidized by air, we used the relative permitivity of tantalum oxide (Ta_2O_5). The total attractive potential is obtained by summing Eq. 7 over the N_c charges in the CD_4 layer. For a selected unitary charge (e.g., an anionic fragment), we have also evaluated the average potential felt by an ion when it moves from its initial position to 20 nm perpendicular to the surface along the z-axis. This somehow mimics the desorption of any stable anion (i.e., B^-) from the CD_4 film. The case of a 1 ML sample is sketched underneath in Fig. 1. For simplicity, in this figure and the following calculations, we neglect any positive charges that may arise from DD. This contribution is considered to be negligible, since within the investigated energy range, the cross section of this process is nil or very small; in any case, DD creates essentially cancelling negative and positive charges within a usually small volume.

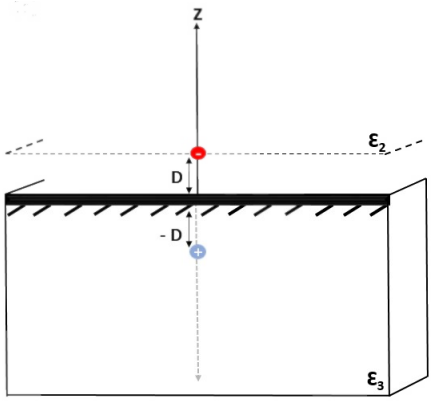

Figure 1: Descriptive scheme of the negative charge Q (in red) formed in a CD_4 monolayer (ε_2) and its image charge -Q (in light blue) induced in the substrate (ε_3).

The potentials between the selected unitary negative charge (the desorbing anion) and the other fixed repulsive charges in the layer, as well as the attractive image charges from the metal were calculated at each step of 1 Å. This instruction was repeated for all N_c charges. The simulation was applied for different numbers of charges (N_c=2, 3, 7, 10, 13, 15, 19, 25 charges) present in the 625 deuterated methane molecules per monolayer, thus aiming at determining the evolution of the total potential as a function of the surface charge ratio, respectively θ_c= 0.32, 0.48, 1.12, 1.60, 2.08, 2.40, 3.04, 4.00 % associated to the different N_c values. 1000 repeated random generations were performed to account the charge distribution. The potential obtained by averaging the total potentials calculated at each random throw becomes afterwards the average total potential per charge. From a statistical point of view, for the various charge configurations, 1000 simulations were found to be sufficient to obtain a stable result as the modeling error converged.

2.3. Adsorption energies

In order to better understand the adsorption competition between a water molecule and deuterated methane on different metal substrates, an adsorption energy calculation was performed for these two molecules, both on the platinum and oxidized tantalum surfaces by using the Vienna ab initio Simulation Package (VASP) software. The plat-

inum (111) structure is formed by 3 layers with unit surface of 4×4 for each of them. The tantalum (110) structure is constituted of 4 layers with unit surface of 4×4. The Ta atoms in the last layer have been replaced by oxygen atoms to form the O/Ta structure. We used the geometric configuration suggested by Guo et al. [33]. The substrate atoms (Pt or O/Ta) were allowed to relax during the energy calculations of the system. The substrate slabs are separated by a 70 Å vacuum region from their periodic image to avoid any interaction between them along the normal direction to the surface. The wave functions of the valence electrons consist of plane waves with a cutoff kinetic energy of 600 eV. The core electrons are treated by the PAW (Projector Augmented Wave) pseudopotential method [34]. The exchange and correlation function used are the revised Perdew-Burke-Ernzerhof functional (revPBE) [35, 36]. Correction for long-range interactions was also considered using the Grimme (-D2) method. The k-point grid was sampled by 5×5×1 with a Fermi level gap of 0.2 eV using the Methfessel-Paxton scheme. Total energy calculations were performed with the Davidson block iteration method for electronic relaxation. The electronic energies were considered to converge as soon as the force on each atom was less than 10^{-3} eV/Å.

The total energies of the substrate with the adsorbate molecule in the ontop position on the surface (above the Pt or Ta substrate atom), the clean surface, and the gas-phase molecule X (H_2O or CD_4), were calculated to obtain the adsorption energy from the following expression:

$$E_{ads}(X) = E(X/Substrate) - E(Substrate) - E(X). \tag{8}$$

Substrate is for Pt or O/Ta.

3. Results

3.1. Numerical simulation results

Total average potential for 1 ML CD_4.

Figure 2 represents the total potential calculated for various charge ratios θ_c in a single CD_4 monolayer deposited on a gold substrate. It clearly demonstrates that except at extremely small distances from the substrate and at very low surface charge ratio (θ_c), the total average potential is repulsive (Fig. 4).

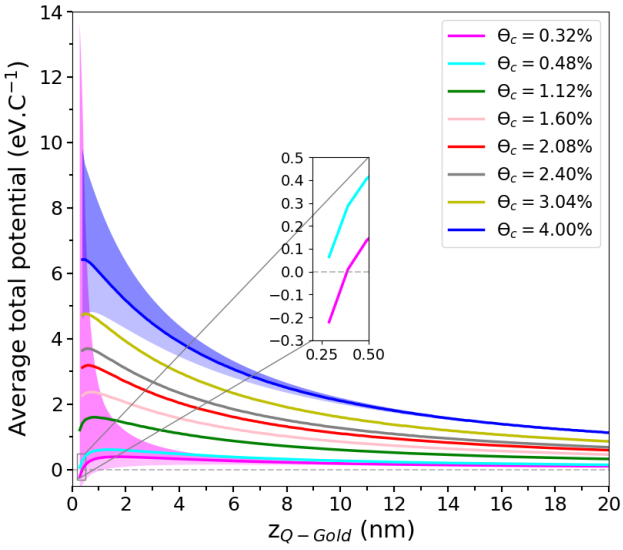

Figure 2: Average total potential as a function of the distance to a gold substrate for a CD_4 monolayer with various surface charge ratios (See legend). The inset show a magnification of the two potential curves (θ_c= 0.32 and 0.48%), where the total potential is attractive only for distances < 0.35 nm and θ_c < 1.12%. The blue and fuchsia zones along the potential curves represent the largest deviation from the average potential observed all along the 1000 calculation runs.

The trend is the same for 1 ML CD_4 with $0.34 \leq \theta_c \leq 4.00$ % deposited on Ta or Pt (not shown). It thus appears that within a CD_4 monolayer with $\sim$ 0.4 nm thickness, irrespective of surface charge ratio > 0.32 %, a D^- ion produced following a DEA process within the layer, experiences a repulsive force, which may thus help enhancing the ESD yields. In such a situation, the term -βE_{pol} in Eq. 4 is positive and there is a gain in kinetic energy. The collective effect of 2 to 25 charges ($0.32 \leq \theta_c \leq 4.00$ %) studied over the complete set of 625 CD_4 molecules in the monolayer is therefore increasingly repulsive as the charge fraction increases and can reach several eV.C^{-1}. Our main objective with this study is to interpret the shifts and special features observed experimentally (especially those shown Figure 6). Ta is known to oxidize readily to various oxidation states and the oxides occur in amorphous and crystalline states. This is not the case with gold. That is why we used, on the one hand Ta_2O_5, and pure gold on the other hand. We present in Fig.3 the average repulsive, attractive and total potentials

determined for 1 ML CD_4 on Au and Ta surfaces, when N_c = 2 (θ_c=0.32 %).

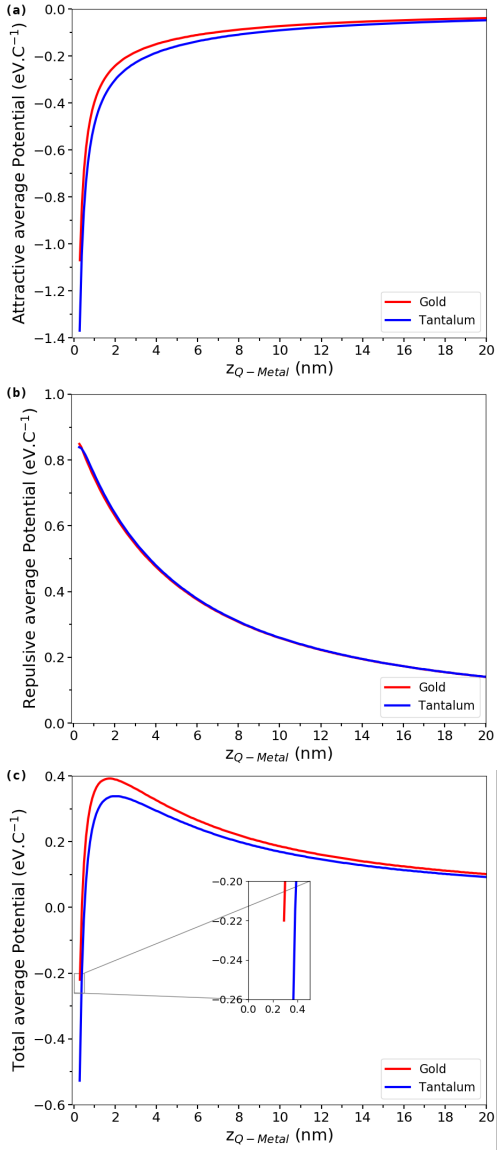

Figure 3: Respectively from up to bottom; average attractive (a), repulsive (b) and total (c) potentials as a function of the distance z_Q from gold, or tantalum substrates for a CD_4 monolayer with surface charge ratio θ_c= 0.32 %. The insert shows a magnification of a portion of the region where the total potential is attractive at very short distances.

255 The total average potential is repulsive for all the distances greater than $\sim$ 0.3 nm

and necessarily more repulsive when the surface charge ratio > 0.32%. Furthermore, as the relative permittivity (ε_3) of the substrate decreases, the average total potential increases. At large distances from the surface, the repulsive potential tends to 0.1 eV.C^{-1}, while it peaks at $\sim$ 0.35 – 0.40 eV.C^{-1} near z_Q = 2 nm. The repelling potential acting on a unitary negative charge, such as a desorbing anionic fragment is thus rather significant. Adsorption forces due to the presence of metallic substrates were not considered in our model, since their effect seems negligible beyond a few CD_4 monolayers from the data presented in Fig. 5. We therefore anticipate that contaminants which can be present on the gold and tantalum substrates, depending on their amount, may hide the influence of such forces between the metallic surface and the CD_4 molecules (see below).

Forces acting on an anion at different depths in the CD_4 sample.

In this section, we look at the influence of charge distribution in multilayered samples, as charges may both push or pull anions produced immediately after the fragmentation of the CD_4^{-*} TNI. The total electrostatic potentials depend on the z-coordinate of the fragment in the layer, but cannot give sufficient information due to their scalar nature. By contrast, the force acting on a given charge within a CD_4 film provides directional information on how coulombic interactions may help extracting anions from the sample layer. In Fig. 4, we present the average total force acting on a unitary negative charge placed in the first, second or third CD_4 monolayer deposited on a gold substrate for θ_c=0.32 %. A negative force indicates that anionic fragments experience an attraction toward the gold surface; conversely repulsion occurs when it is positive. Within the first and second layers, the total force appears to be such that an anion created in those layers first experiences an attraction toward the metal surface. It can be deduced from Fig. 3 that within a CD_4 monolayer with θ_c=0.32 % at 0.25 nm from the surface, the total potential is rather weakly attractive and equal to - 0.2 eV.C^{-1}. For two CD_4 layers and still θ_c=0.32 %, an anion produced within the second layer again experiences attraction. From Fig. 4, it can be observed that for an anion in the third layer, interactions are repulsive and thus help overcoming the charge-induced polarization barrier of the substrate and hence increase the kinetic energy perpendicularly to

the surface. An anion located at the interface 2 ML – 3 ML experiences two repulsive forces which compensate each other (one from the first ML and the other from the 3^{rd} ML) with an additional attractive force from the substrate (image force). An anion located in the first ML will experience an attractive force stemming from the substrate (image) and a repulsive force from the two external layers that add up (ML 2 and 3). As for an anion in the third ML (the farthest from the substrate), it will experience two repulsive components both directed towards the vacuum and one attractive force (image). Comparison between the total average potentials presented in Figure 3 and in Figure 4 (inset) for gold must be carried out with care. Although both figures are for the same surface fraction θ_c, in Figure 3, only one ML is considered as Figure 4 is for 3 ML. Therefore, an anion that resides in the first ML covered with two supplementary stacked ML will feel the repulsion of negative charges present in these layers. In that case the repulsion prevents its desoprtion out of the layers. This is illustrated in Figure 4, where the forces rather than the potentials are shown. We found that this behavior was repeated for 4 CD_4 ML and additional layers (not shown). This proposal is valid for θ_c=0.32 %, if the surface charge ratio increases, repulsive forces will also act in the two first layers. It is important to keep in mind that several additional parameters (Eq. 5) may affect the value of anions kinetic energy. It should be noted that the inset in Fig. 4 shows the potentials, but the figure itself shows the force (the gradient of the potential). This is very convenient because the sign of the force indicates if the anion is pushed out (positive force) or attracted to the substrate (negative force).

3.2. Experimental results

Experimental evidence of the role of the substrate and its purity on ESD and DEA.

To illustrate experimentally the effect of the type and purity of the substrate on the ESD yield functions, monolayers (ML) of CD_4 were deposited on Pt, Ta and Au substrates. Only the Pt substrate was cleaned by heating to redness in the vacuum chamber. The tantalum and gold substrates were not heated and may possibly be soiled with atmospheric pollutants which are generally composed of secondary inorganic compounds (such as NH_4HSO_4 and NH_4NO_3), organic alkyl compounds (like aliphatic compounds), and nitrogen-containing organic compounds [37], most of them being re-

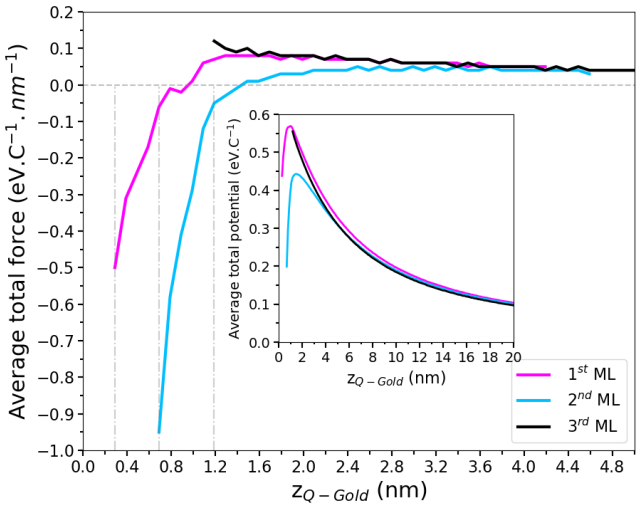

Figure 4: Average total forces acting on a unitary negative charge as a function of the distance z_Q from a gold substrate when the charge resides in one of the 3 CD_4 MLs indicated in the right bottom corner. The surface charge ratio is θ_c= 0.32 % and a supplementary negative charge is randomly distributed all over the 3 MLs. The average total force comes from 1000 samplings of the additional negative charge. The three vertical dashed lines in light grey correspond to the interfaces between the 3 MLs. The inset shows how the average total potential evolves with the distance z_Q from the gold substrate for an anion localized in the 1st, 2nd or 3rd CD_4 ML.

leased in the atmosphere as particles by the combustion of fossil fuels. It should be noticed that such pollutants, if present, are under the form of particles, not layers. In addition, when the Au and Ta substrates are cooled down to $\sim$ 15 K in vacuum to adsorb the CD_4 layers, residual water was also adsorbed onto the surface prior to CD_4 deposition. Contrary to atmospheric pollutants, water can arrange from monomer to ice adlayers on the surface; with possibly both oxygen and hydrogen bonding on single crystal-metal surfaces [38, 39]. In the present study, this is not considered to be the case for the Pt surface, which is covered by CD_4 immediately after cooling of the clean substrate in ultra-high vacuum.

We first focus on experiments where 2 MLs of CD_4 were successively deposited on each of the three substrates. With all other parameters being equal during ESD experiments, it appears clearly on Fig. 5 that when one ML of CD_4 was deposited on clean Pt, DEA to CD_4 (i.e., $CD_4 + e^- \rightarrow CD_4^{-*} \rightarrow CD_3 + D^-$) is inhibited, whereas for

deposition on contaminated Au and Ta substrates the anion signals are much stronger. It should be noticed that with 1 ML CD_4 on Pt, the DEA peak spreads to higher electron energies possibly due to multiple energy losses by electrons backscattered from the metal (pink arrow on Fig. 5a). For a second ML deposited on platinum, the DEA peak then slightly appears near the expected energy and further increases in amplitude with additional layers to peak at an energy of $\sim$9 eV (See Fig. 6a). For tantalum and gold, the resonance peak is clearly apparent with 1 ML, and its amplitude increases with additional MLs, with a trend toward saturation as shown in Fig. 6.

At a first glance, it is surprising to observe that contaminated substrates provide rather large desorption yields when covered with very small CD_4 thicknesses, while this is not the case for the clean one (Pt). It is understandable since, when a CD_4 molecule is adsorbed on a clean metal surface, its potential energy surfaces (PESs) and those of its TNI manifold are modified. Although, in the case of physisorption, the relatively small perturbation of the ground and excited neutral states may not be pertinent, those of the TNIs are significant. The TNIs states are formed at lower energies, due to induced charge polarization when physiosorbed on a metal surface, and they are further modified by the probability of electron transfer to the metal. These phenomena modify the lifetimes of TNIs and increase the number of its decay channels [8]. Their combination decrease DEA yields [8]. Conversely, with a contaminated surface, these effects are considerably reduced, if not negligible, since the CD_4 layers are remote from the substrate surface. Details of the consequences of substrate proximity on the intrinsic properties of TNIs and DEA are not treated herein but will be considered in a forthcoming article.

It appears clearly that the threshold energies of the D^- signal (TEs), the peak energies (PEs) and ESD yields for the desorption of D^- ions are substrate-dependent. There are several possible explanations for the observed differences in yield functions. They might all be related to the adsorption phenomena, i.e. $E_{B^-/S}$ and $E_{AB/S}$, which occurs for ions and the parent molecules, to electrostatic interactions E_{B^-/Q^-}, as shown in Eq. 5 and to effects related to the thickness of the layers, especially multiple collisions of both desorbed ions and incident electrons. Electron attachment and detachment on

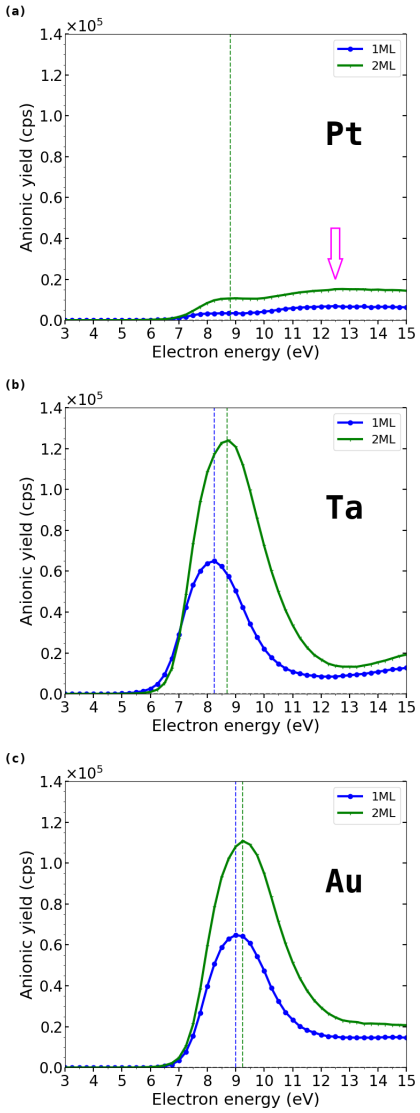

Figure 5: Yields functions for the desorption of D^- ions from 1 and 2 ML of CD_4 deposited on clean platinum (a) and contaminated tantalum (b) and gold (c). Dashed vertical lines are drawn to determine the peak energies and horizontal ones to compare the heights of the resonance peaks. For the pink arrow in (a), refer to the text.

the parent adsorbed molecule can also be tuned somehow by the substrates. We also find an increase of the PEs in passing from 1 ML to 2 ML.

Experimental evidence of CD_4 layer thickness influence on ESD/DEA.

Desorption yields have been experimentally measured for various CD_4 thicknesses, namely for 1 to 5 ML deposited on Ta and Au substrates and from 1 to 12 ML on platinum. Data obtained for the platinum substrate are presented on the up side of Fig. 6, in the middle for the tantalum substrate, while those for gold are shown on the bottom. The characteristic values of the yield function obtained for D^- ESD from CD_4 physisorbed on the Pt substrate with various CD_4 thicknesses are listed in Table 1, those corresponding to the Ta and Au substrate are respectively gathered in Tables 2 and 3. The most striking feature is the different trend of the platinum yield function compared to those of the other two substrates, which are similar. This means that the interactions within the adsorbed layers, i.e. $E_{B^-/Q}$ and E_{B^-/Q^-} become dominant with the Au and Ta substrates, as shown by Eq. 5.

Table 1: Characteristic values of the yield function obtained for D^- on the platinum substrate with various CD_4 thicknesses. TE is the threshold energy, PE is the peak energy and Yield in the last column represent the area under the peaks in the interval [3-15] eV.

Thickness (ML)	TE (eV)	PE (eV)	Maximum yield (cps)	Yield (10^5 cps.eV)
1	6.20	9.00	2649	0.50
2	6.20	9.00	8176	1.17
3	6.20	9.25	20333	1.69
4	6.50	9.25	36452	2.00
5	6.50	9.50	51126	2.06
6	6.50	9.50	61830	2.21
9	6.70	9.75	74264	2.59
12	6.80	9.75	78836	2.76

Concerning these two substrates, as the CD_4 film thickness increases, we find that: i) the magnitude of the DEA peak increases; ii) the DEA peak broadens; iii) the TEs shift to higher values; iv) the TEs follow the same trend as that of the PEs; v) the height

Table 2: Characteristic values of the yield function obtained for D^- on the tantalum substrate with various CD_4 thicknesses. TE is the threshold energy, PE is the peak energy and Yield in the last column represent the area under the peaks in the interval [3-15] eV.

Thickness (ML)	TE (eV)	PE (eV)	Maximum yield (cps)	Yield (10^5 cps.eV)
1	5.2	8.25	65071	2.16
2	5.5	8.75	123961	4.20
3	5.75	9.0	138810	4.95
4	5.75	9.0	144073	5.25
5	6.0	9.0	145727	5.24

Table 3: Characteristic values of the yield function obtained for D^- on the gold substrate with various CD_4 thicknesses. TE is the threshold energy, PE is the peak energy and Yield in the last column represent the area under the peaks in the interval [3-15] eV.

Thickness (ML)	TE (eV)	PE (eV)	Maximum yield (cps)	Yield (10^5 cps.eV)
1	5.9	9	64768	2.33
2	5.8	9.25	110808	4.04
3	6	9.5	126153	4.49
4	6.2	9.5	136123	4.87
5	6.2	9.5	139189	5.08

of the DEA peaks follows a specific trend, namely when passing from an "n-layer" to the (n+1)-layer thickness; the difference in consecutive peak heights decreases as "n" increases, causing the saturation in the yields, shown by the red curves in the insets of Fig. 6. The latter trend is the same for the peak areas as seen from the blue curves in these insets. This saturation appears thus to be an indisputable trend for all substrates. The TEs vary differently for the two substrates, i.e., ΔTE_{max}=0.4 eV for Au and 0.8 for Ta, as well as the PEs (ΔPE_{max}=0.5 eV for Au and 0.75 eV for Ta) with respect to the thickness of the CD_4 samples. It is worth mentioning that electron energies are experimentally sampled using constant steps of 0.25 eV. The broadening of the peaks

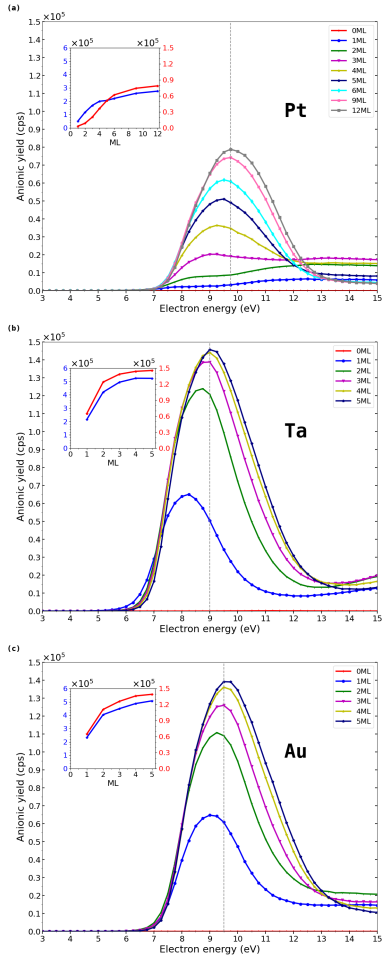

Figure 6: Yield functions of D^- ions from 0-12 ML of CD_4 deposited on platinum (a), 0-5 ML on tantalum (b) and 0-5 ML on gold (c) substrates. The gray dashed line is drawn to guide the eye; it highlights how the DEA peak energies shift to higher values with increasing thickness. The curves in the insets show the yields (cps.eV) on the left axis (in blue) and the maximum yields (cps) of the peaks on the right axis (in red). They were constructed from the data in Tables 1, 2 and 3; they illustrate the saturation in ESD yields observed with all substrates.

as well as the shift in TEs and PEs to higher energies might possibly be reminiscent of a probability distribution function of electron collisions. If we state that TEs and PEs should be insensible to the thickness of the layers, then we can interpret the shifts as a consequence of the amount of electron energy loss prior to DEA; namely ΔE_i in

Eqs. 4 and 5. Obviously, the electron scattering probability in the deposited films increases with film thickness (see the discussion section). Thus, in the thicker films, there is inevitably a larger decrease of the average electron energies. In other words, since electrons undergo increased scattering within thicker films, they lose more energy on average and hence the DEA peak broadens and the TE shifts to higher values. The same applies to the tantalum substrate. That is the reason why we observe broadening, as well as TE and PE shifts in Fig. 6 with film thickness. This point is examined in more details in the discussion section.

The second observation is that the maximum anionic yield tends to plateau, as a function of the number of CD_4 MLs. Such a saturation exhibits a logistic pattern from 1 to 5 ML, reminiscent of a phase-transition process. Indeed, the first monolayer is actually a 2-D nanosystem, which gradually expands into a 3-D nanosystem. Five MLs corresponds typically to a 2 nm thickness. This transition progressively includes the effects of the incoming electrons energy losses prior to DEA and the collisions experienced by the ions produced via DEA; namely the terms ΔE_i and E_{B^-/Q^-} as well as $E_{B^-/Q}$ in Eq. 5. The effect of the first term (ΔE_i) on the yield functions has at least partly been explained above. The loss of kinetic energy by the anion due to collisions with adjacent molecules in the layer is obviously a growing function of the layer's thickness. It is thus clear that for layer thicknesses which exceed 5 ML, a part of the anions formed near to the metallic surface (deep inside a multilayer) may not be able to escape out of the sample and thereby would increase the charge ratio (see the discussion section for a quantitative description).

4. Discussion

Before going into further details, it seems mandatory to quantify as precisely as possible the role played by scattering of both desorbed anions and incoming electrons in the samples. The data presented in Figs. 5 and 6 indicate that the resonances peak typically near to 9 ± 1 eV, whatever is the metallic substrate used and the number of CD_4 ML. Computation of both dissociation energy, D_0 and electron affinity, E_a have been performed at the DFT-B3LYP/6-31+G(d,p) level of the Gaussian computational

chemistry software package [40], in order to determine the kinetic energy of Eq. 3 of the desorbed anion in $CD_4 + e^- \rightarrow CD_4^{-*} \rightarrow CD_3 + D^-$. The dissociation energy into neutrals was computed as the difference between the total optimized energy of the neutral CD_4 molecule and the sum of the optimized total energies of each neutral fragment (CD_3 + D). This gave the value of D_0 = 4.87 eV. A value of 4.48 eV, close to the one we obtain was recently published for the dissociation energy of H-CH_3, which is by 8% lower than our result [41]. The electron affinity was determined as the difference between the optimized total energies of neutral and anionic states of the fragment; the result for the deuterium atom is E_a = 0.75 eV. This results is in perfect agreement with data published by others, namely exactly the same value; 0.75 eV [42]. By using Eq. 3 and neglecting the excitation energy, we get the following value for the kinetic energy of a desorbed fragment (in the vacuum), T_{D^-} = 4.39 eV. As we ignore the value of the excitation energy E^*, the estimated kinetic energy overestimates somewhat the exact value. Regrettably, there is no published cross section data for momentum transfer in the D^-/CD_4 system. The closest cross section we found is the H^-/H_2 one [43], which for T_{H^-} = 4.39 eV is $\sigma = 4.6\times10^{-16}$ cm^2. We use the relation $J = J_0 \exp(-n_0\sigma x)$ to estimate the transmission probability $P(x) = J/J_0$ of D^- (H^-) anions through a thickness x, in which n_0 stands for the number of CD_4 molecules per cm^3. With 625 deuterated molecules having a diameter of 4 Å covering an area of (100 $\times$ 100) Å, the molecular density of the films can be estimated to $n_0 = 1.56\ 10^{22}$ cm^{-3}. The relation mentioned above is generally used for experiments based on ion–neutral collisions at low energies [44]. With a ML thickness of 4 Å, the transmission probabilities are respectively 75 %, 56 %, 42 %, 32 %, 24 % and 18 % for 1 to 6 ML. Less than half (42 %) of the desorbed anions are for example transmitted through a thickness equivalent to 3 ML and less than 1 D^- ion over 5 (18 %) may cross a 6 ML thickness. As the CD_4 molecule is much larger than H_2, it is likely that the cross section for momentum transfer in the D^-/CD_4 system is larger than those in the H^-/H_2 one, at a same energy. It should be noticed that starting from 4.98 eV, when the energy of the H^- ion decreases (due to scattering), the cross section increases, therefore after each momentum transfer, a desorbed ion has an increasing probability to be scattered again. Therefore the transmission probabilities given above are in fact overestimations. When the anion is slowed down so its energy

reaches 2 eV, $\sigma = 10^{-15}$ cm^2, P(x) = 0.54 for 1 ML and P(x) $\rightarrow$ 0 for 6 ML.

For low energy electrons, the transport mean free path λ_{tr} is related to the transport cross section by λ_{tr}= $(n_0\ \sigma_{tr})^{-1}$ [45], we can use the same relation (a Poisson distribution, i.e. J=J_0 exp(-$n_0\ \sigma$ x) to estimate the electron beam attenuation and thus the transmission probability through CD_4 layers. In the [1-10] eV energy range, total scattering and momentum transfer (also called momentum-transport) cross sections are almost equal in methane [46]. The momentum transfer cross section for electrons incident on CH_4 is characterized by a maximum in the energy range [6 - 10] eV; this maximum corresponds to a cross section value within the interval [1×10^{-15} - 2×10^{-15}] cm^2, depending on the authors [47]. We will use the average $\sigma = 1.5 \times 10^{-15}$ cm^2. With this value, we get respectively the following transmission probabilities when passing through 1 to 6 ML: 39 %, 15 %, 6 %, 2 %, 1 %, 0.4 %. Electrons are thus more attenuated by the CD_4 layers than D^- ions. In addition, contrary to H^- ions, electrons have momentum transfer cross section that drastically decrease when the energy decreases in the [10 – 1] eV range [47]. This decrease being of two orders of magnitude in the cited energy range, this means that, in comparison with electrons that leave the gun, those which have suffered momentum transfer in the first CD_4 layers will be increasingly less attenuated as they move to the following layers. On the contrary, higher energy electrons ($T_{e^-} > 9$ eV), when they are slowed down, first experience an increase of their cross section up to 8-9 eV, where the cross section for momentum transfer peaks. Lastly, for samples with thin coverage (i.e. with few ML), a given proportion of the incident electrons is prone to cross the CD_4 layers, then to enter the metallic substrate where they can be scattered. The work functions for platinum is 6.35 eV, 4.1 eV for tantalum and 5.1 eV for gold. Incident electrons which enter one of these metallic substrate with higher energies may be able to produce secondary electrons. Those latter, nevetheless, may have to small energies to attach to the CD_4 molecules via resonant processes. This confirms that all processes experienced by electrons ultimately contribute to ESD peak broadening when the thickness increases. At a given depth in the layer, the incident electron energy E_i has been reduced due to scattering but the desorbed anion yield will be recorded on the spectrum at E_i. This explains why

peaks broaden to larger energies when the thickness increases (Fig. 6). As for desorbed anions, our estimates clearly highlight that with the exponential decay of the transmission probabilities, the yield of desorbed D^- ions must drastically drop down when a few ML have to be crossed. This especially because the cross section for momentum transfer increases when the kinetic energy of the anion decreases. It is therefore not surprising that the yield functions (especially those for gold and tantalum substrates) in Fig. 6 exhibit a plateau behavior when the number of monolayers exceeds 5 to 6 ML. We may state that the 5-6 external ML at the vacuum interface are the active layers for ESD, those located deeper will experience DEA but the probability that desorbed anions escape out of the thick layer will be extremely low. The curves in the insets in Fig. 6 comply with this statement. But ESD data for the platinum substrate, at least for small numbers of ML, deviate from these rules.

It becomes increasingly clear that with yield functions features, as those presented in Fig. 5, the Ta and Au surfaces must be covered with contaminants which play a role similar to the first few CD_4 layers on Pt, as shown in Fig. 4. Atmospheric contaminants being generally under the form of micro particles, it is unlikely that they entirely cover the surface. However, it is possible that water rather than other atmospheric contaminants is significantly present on the surface. The presence of water on Ta and Au is indeed confirmed by ESD data (Fig. 7a) of H^- from 1 ML CD_4 deposited on Pt, Ta and Au metallic substrates. Desorption yields for H^- anions are substantial for Ta and Au substrates, especially since they have to cross the external CD_4 layer, which should reduce their desorption. In Figure 7b, we show the region of the TE for peaks relative to H^- desorption. Three different signals are gathered in this figure; namely for two gold substrates which have been analyzed at 15K and 300K and a gold substrate covered in the vacuum with 1 ML H_2O at 15K. It is clear from Figure 7b that all H^- signals have the same TE, thus confirming that water already is present on the gold substrates. Because of the similarity of the signals observed in Figure 7a, we will assume that tantalum substrates also are covered with adsorbed water. The number of adsorbed layers was not determined herein, nevertheless all indications are that this number of adsorbed layers is small, most likely less than 3 ML.

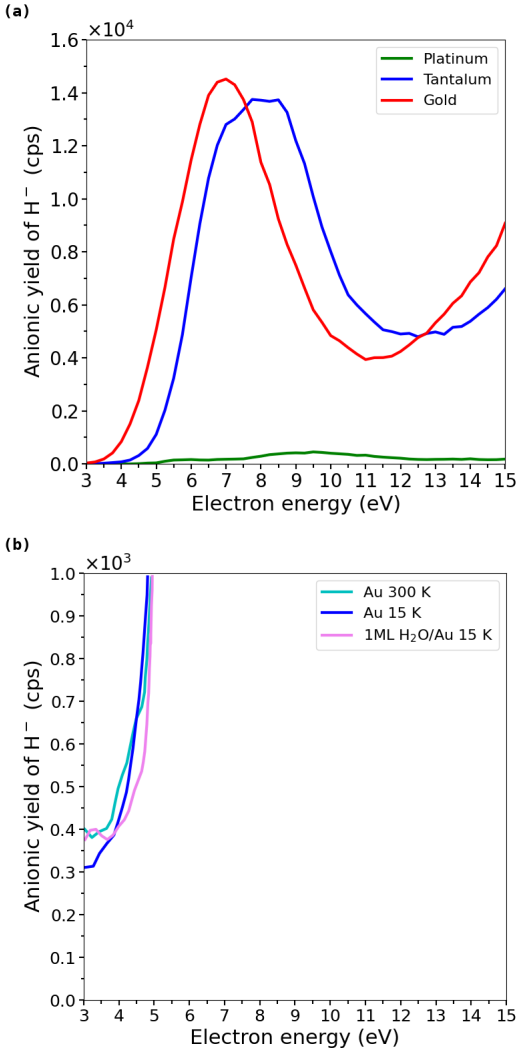

Figure 7: H^- ESD yields for 1 ML CD_4 deposited on clean platinum, contaminated gold and tantalum surfaces (a). Enlargement of the TE region for ESD of H^- relative to three gold substrates. ESD measurements for the samples have been realized either at 300K or at 15K. For the two samples kept at 15K, one was covered with 1 ML H_2O in the vacuum prior to ESD analysis (b).

In order to compare the relative magnitude of the adsorption of H_2O and CD_4 on Pt and O/Ta, a model has been proposed, which enables adsorption probabilities to be

computed. The gold samples were not included in these calculations due the difficulty to model their surfaces. Gold surfaces are indeed known to be characterized by surface reconstruction (distortions such as reconstructed facets, expansions and steps) [48]. Interestingly however, using Scanning Tunneling Microscopy under Ultra High Vacuum, it was shown that water adsorption on gold proceeds via a weak interaction and leads to a unique double bilayer formation [49].

The relative adsorption energies (difference in adsorption energies between H_2O and CD_4 molecules) on a same substrate (denoted "i"), at the same position (on top position for the present calculations) is defined as:

$$\Delta E_{ads}^{(i)} = E_{ads}^{(i)}(H_2O) - E_{ads}^{(i)}(CD_4) \tag{9}$$

The adsorption probability of H_2O expressed with respect to that of CD_4 is:

$$P_{H_2O}^{(i)} = \frac{e^{-\alpha E_{ads}^{(i)}(H_2O)}}{e^{-\alpha E_{ads}^{(i)}(H_2O)} + e^{-\alpha E_{ads}^{(i)}(CD_4)}} \tag{10}$$

where α=$\frac{1}{k_B T}$

A simple transformation produces the H_2O adsorption probability:

$$P_{H_2O}^{(i)} = \frac{1}{1 + e^{\alpha \Delta E_{ads}^{(i)}}} \tag{11}$$

The adsorption probability of CD_4 on the same substrate "i", is thus:

$$P_{CD_4}^{(i)} = 1 - P_{H_2O}^{(i)} = \frac{1}{1 + e^{-\alpha \Delta E_{ads}^{(i)}}} \tag{12}$$

Adsorption energies for H_2O when the 2 hydrogen atoms are oriented toward the surface have been compared with the case where the oxygen atom is oriented toward the surface. The first case had the highest adsorption energy (in absolute value) and was selected. As for CD_4, the two situations were considered, namely when one deuterium atom is oriented in direction of the surface or when three of them are in direction of the metal. The last one was selected for its highest adsorption energy (in absolute value). Calculation of probabilities have been performed both at ambient (300 K) and cryogenic (15 K) temperatures, results are presented in Table 4. For more comprehensive information, the reader is referred to the "Adsorption energies" part of the materials

Table 4: Calculated relative adsorption energies ΔE_{ads} (meV), adsorption probabilities P, at 300 K and 15 K for H_2O and CD_4 molecules on platinum and oxidized tantalum.

Substrat	$\Delta E^{(i)}_{ads}$	$P^{(i)}_{T=300K}$		$P^{(i)}_{T=15K}$	
		H_2O	CD_4	H_2O	CD_4
Pt	30	0.24	0.76	0	1
O/Ta	-120	0.99	0.01	1	0

and methods section.

ΔE_{ads} Eq. 9 is positive for Pt and negative for O/Ta; therefore, water has a much higher propensity to adsorb on O/Ta than on platinum. Conversely adsorption of CD_4 is prevailing on platinum. At the cryogenic temperature of 15 K used in our experiments, adsorption probabilities are such that water adsorption on O/Ta almost excludes CD_4 while on platinum, CD_4 adsorption is fully preferred. In order the data in Table 4 is clearly understood, it may be mentioned, as an example, that the adsorption probability of water on Pt at 15 K is 10^{-17}. The determined adsorption energies and probabilities not only agree with the hypothesis of water layers adsorbed on O/Ta. The adsorption data also demonstrate that if water and deuterated methane are in competition for the formation of adsorbed layers, it is the CD_4 molecule that preferably adsorbs on a clean platinum surface. Hence, these results are shedding new light on Tables 1-3 and Figs. 6a-c. tantalum and gold surfaces were not heated and cleaned prior to CD_4 deposition while the platinum substrate was heated in the vacuum chamber. As a result, the residual water molecules in the vacuum chamber are in competition with the CD_4 molecules for the cryogenic condensation on the different metallic substrates. Whereas H_2O is likely to condense on the O/Ta substrate, CD_4 is preferably adsorbed on platinum. Even if we didn't measure precisely the number of adsorbed ML of water, there is evidence that H_2O adsorbs prior to CD_4 molecules on O/Ta and thus provide a supplementary thickness of condensed matter between the substrate and the external CD_4 layer(s). Lastly, with ε_2 = 80 at 20°C for water instead of ε_2 = 1.1 for a CD_4 layer, the attractive forces should be drastically lowered Eq. 7, which reinforces the

argument that adsorbed water between the surface and the CD_4 layers may enhance ESD of D^-. Conversely platinum is immediately covered with CD_4 molecules, and those latter are undoubtedly strongly adsorbed, causing important perturbations to the transient negative ion (CD_4^{-*}) and to the further dissociation step; as can be observed on Fig. 6a. On this Figure, the yield functions corresponding to 1, 2- and 3- ML show indeed anomalous features, notably a broad spread of the resonance to the higher energies. Such behavior is completely absent in both yield functions of tantalum and gold substrates, where adsorbed water at the substrate surface plays the role of a high dielectric constant screen.

5. Summary and conclusion

As shown experimentally with the clean Pt surface, the desorption yields of D^- ions from a CD_4 layer is drastically reduced and the yield functions appear impaired for 1-3 ML (Fig. 6a), when compared to the signals stemming from O/Ta and Au surfaces (Figs. 6b and c). This is due to the contamination layer(s) of water which are present on the O/Ta and Au substrates. Furthermore, ESD yield functions of CD_4 multilayers deposited on the 3 surfaces exhibit a common behavior; namely, the D^- resonance peaks broaden when the number of MLs increases and their area and height follow an S-shaped curve when reported versus n, the number of MLs. When comparing the different types of metallic substrates used TEs and PEs are nevertheless substrate-dependent (Tables 1-3 and Figs. 6a-c).

Computation of the average total force acting on a unitary negative charge located in the first, second or third layer deposited on a gold substrate (Fig. 4) when θ_c=0.32 % for a 3 ML thickness, has shown that when localized in the first and second layers, anions are weakly attracted while they are pushed out when located in the third layer. Anions would of course also be pushed out if located in the next outer layers, i.e. n > 4. This result can be extended to the case of tantalum substrates on which water also is adsorbed. As we observe a well-defined resonance as early as 1 ML is deposited on both Ta and Au substrates, we therefore conclude that water plays a role equivalent to $\sim$2 CD_4 layers. Adsorbed water increases the vertical distance between the metallic

surface and the CD_4 layers in such a way that ejection of anions is promoted by repulsive forces. Besides, those later forces are increased for a water layer due to its high relative permittivity.

Our calculations also show that the concept of a charge-induced average polarization barrier which must be overcome by the anion fragment during desorption (E_{pol}) only stands for special cases (low surface charge fraction and extremely thin layers).

The initial kinetic energy of the anionic fragments and their possible slowing down when passing through a molecular layer are essential parameters to fully understand the features of experimental ESD yield functions, especially when dealing with thick layers ($E_{B^-/Q}$). Electron collisions also must be considered. they correspond to the term ΔE_i. The broadening of the resonance peaks observed when increasing the layer's thickness is due to a compensating effect between kinetic energy losses (collisions experienced by the anionic fragment) and the repulsive potential which can (at least partly) offset the energy losses of desorbed anions. With an S-shaped curve: area (or height) of the peaks versus number of ML (insets in Figs. 6a-c), this intricate compensating effect is such that the desorption rate attains a plateau value for large numbers of ML (typically > 6). Overall, the features described are reminiscent of a 2-D to 3-D transition.

Interestingly, the present study underlines the fact that samples soiled with water (herein O/Ta and Au), which are commonly used in numerous ESD experiments, present the advantage of highly promoting the desorption of anions even when covered with few ML.

Lastly, in this study, surface interactions of both parent molecule and generated fragments (physisorption and chemisorption) were not considered ($E_{B^-/S}$) Such interactions ought also to play an important part in the bulk desorption process, especially for clean surfaces such than platinum and thus alter the final feature of an ESD yield function (Fig. 5a and 6a). It has for example been measured [32] and computed [37] that neutral fragments (H, CH, CH_2 and CH_3) when adsorbed on platinum have adsorption energies (E_{ads}) varying from -2.04 eV (CH_3) to -6.43 eV (CH). Such energies irrefutably indicate that strong adsorption phenomena arise on metallic substrates; incorporating chemisorption and therefore possible chemical reaction between the surface and the adsorbate. Equation 5 should therefore include the adsorption process in

the $E_{B^-/S}$ term and extend it to adsorption of neutral species. Studies of these surface interactions are currently under progress.

Acknowledgments

The authors would like to thank the Mésocentre de calcul de Franche-Comté, which allowed us to perform several simulations on their supercalculators in the course of this work. The authors also wish to thank Nicola Bertolini, intern at the Department of Nuclear Medicine and Radiobiology of the Sherbrooke University for his unwavering devotion to the ESD experiments.

References

[1] T. E. Madey, History of desorption induced by electronic transitions, Surf. Sci. 299-300 (1994) 824–836.

[2] Electron-stimulated desorption: Principles and applications, Surf. Sci. Rep. 12 (6) (1991) 246–378.

[3] L. Sanche, Dissociative attachment in electron scattering from condensed O_2 and CO, Phys. Rev. Lett. 53 (1984) 1638–1641.

[4] B. Boudaïffa, P. Cloutier, D. Hunting, M. Huels, L. Sanche, Resonant formation of DNA strand breaks by low-energy (3 to 20 ev) electrons, Sci. 287 (2000) 1658–1660.

[5] I. Baccarelli, I. Bald, F. A. Gianturco, E. Illenberger, J. Kopyra, Electron-induced damage of DNA and its components: Experiments and theoretical models, Phys. Rep. 508 (2011) 1–44.

[6] A. N. Sidorov, T. M. Orlando, Monolayer Graphene Platform for the Study of DNA Damage by Low-Energy Electron Irradiation, J. Phys. Chem. Lett. 4 (2013) 2328–2333.

[7] L. Sanche, Low-energy electron interaction with DNA: bond dissociation and formation of transient anions, radicals, and radical anions, in: M. M. Greenberg (Ed.), Radical and Radical Ion Reactivity in Nucleic Acid Chemistry, Wiley Series of Reactive Intermediates in Chemistry and Biology, John Wiley & Sons Inc., Hoboken, NJ, USA, 2009, pp. 239–295.

[8] E. Alizadeh, S. Ptasińska, L. Sanche, Transient anions in radiobiology and radiotherapy: From gaseous biomolecules to condensed organic and biomolecular solids, in: W. A. Monteiro (Ed.), Radiation Effects in Materials, IntechOpen, Rijeka, 2016, Ch. 8.

[9] C. R. Arumainayagam, H.-L. Lee, R. B. Nelson, D. R. Haines, R. P. Gunawardane, Low-energy electron-induced reactions in condensed matter, Surf. Sci. Rep. 65 (2010) 1–44.

[10] B. C. Ibănescu, M. Allan, Selectivity in bond cleavage in amines and thiols by dissociative electron attachment, J. Phys. Conf. Ser. 194 (2009) 012030.

[11] S. Esmaili, A. D. Bass, P. Cloutier, L. Sanche, M. A. Huels, Glycine formation in CO_2:CH_4:NH_3 ices induced by 0-70 ev electrons, J. Chem. Phys. (16) (2018) 164702.

[12] M. C. Boyer, N. Rivas, A. A. Tran, C. A. Verish, C. R. , The role of low-energy ($\leq$ 20 ev) electrons in astrochemistry, Surf. Sci. 652 (2016) 26–32.

[13] I. Bald, J. Langer, P. Tegeder, O. Ingólfsson, From isolated molecules through clusters and condensates to the building blocks of life, Int. J. Mass Spectrom. 277 (1) (2008) 4–25.

[14] H. Sambe, D. Ramaker, L. Parenteau, L. Sanche, Image charge effects in electron stimulated desorption: O^- from O_2 condensed on Ar films grown on Pt., Phys. Rev. Lett. 59 (1987) 236–239.

[15] A. D. Bass, L. Parenteau, M. A. Huels, L. Sanche, Reactive scattering of O^- in organic films at subionization collision energies, J. Chem. Phys. 109 (19) (1998) 8635–8640.

[16] X. Pan, P. Cloutier, D. Hunting, L. Sanche, Dissociative electron attachment to DNA, Phys. Rev. Lett. 90 (2003) 208102.

[17] M. A. Śmiałek, Evaluating experimental molecular physics studies of radiation-damage in DNA*, Eur. Phys. J. D 70 (2016) 237.

[18] Y. Gao, Y. Zheng, L. Sanche, Low-energy electron damage to condensed-phase DNA and its constituents, Int. J. Mol. Sci. 22.

[19] R. Azria, L. Parenteau, L. Sanche, Dissociative attachment from condensed O_2: Violation of the selection rule $\Sigma^- \leftrightarrows \Sigma^+$, Phys. Rev. Lett. 59 (1987) 638–640.

[20] M. H. du Penhoat, M. A. Huels, P. Cloutier, J.-P. Jay-Gerin, L. Sanche, Anion fragment formation in 5-Halouracil films induced by 1-20 eV electron impact, J. Phys. Chem. B 108 (2004) 17251–17260.

[21] P. Możejko, A. D. Bass, L. Parenteau, L. Sanche, Intrinsic and extrinsic factors in anion electron-stimulated desorption: D^- from deuterated hydrocarbons condensed on Kr and water ice films, J. Chem. Phys. 121 (2004) 10181–10189.

[22] M. Bazin, S. Ptasińska, A. D. Bass, L. Sanche, Electron induced dissociation in condensed-phase nitromethane I: desorption of ionic fragments, Phys. Chem. Chem. Phys. 11 (2009) 1610–1618.

[23] M. N. Hedhili, P. Cloutier, A. D. Bass, T. E. Madey, L. Sanche, Electron stimulated desorption of anionic fragments from films of pure and electron-irradiated thiophene, J. Chem. Phys. 125 (2006) 094704.

[24] L. Sanche, G. Bader, L. Caron, Transmission of 0–15 ev monoenergetic electrons through aliphatic and alicyclic hydrocarbon films, J. Chem. Phys. 76 (1982) 4016–4027.

[25] J. Hafner, G. Kresse, The Vienna AB-Initio Simulation Program VASP: An Efficient and Versatile Tool for Studying the Structural, Dynamic, and Electronic Properties of Materials, Springer US, Boston, MA, 1997, pp. 69–82.

[26] G. Kresse, J. Hafner, Ab initio molecular dynamics for liquid metals, Phys. Rev. B 47 (1993) 558–561.

[27] G. Kresse, J. Hafner, Ab initio molecular-dynamics simulation of the liquid-metal–amorphous-semiconductor transition in germanium, Phys. Rev. B 49 (1994) 14251–14269.

[28] G. Kresse, J. Furthmüller, Efficiency of ab-initio total energy calculations for metals and semiconductors using a plane-wave basis set, Comput. Mater. Sci. 6 (1996) 15–50.

[29] G. Kresse, J. Furthmüller, Efficient iterative schemes for ab initio total-energy calculations using a Plane-Wave basis set, Phys. Rev. B 54 (1996) 11169–11186.

[30] P. Malbrunot, J. Vermesse, D. Vidal, T. Bose, A. Hourri, J. St-Arnaud, Determination of densities and dielectric polarizabilities of methane at 298.15 k for pressures up to 710 Mpa, Fluid Phase Equilibria 96 (1994) 173–183.

[31] I. Shklyarevskii, P. Pakhomov, Separation of contributions from free and coupled electrons into real and imaginary parts of a dielectric-constant of gold, Opt. Spectrosc. 34 (1973) 163–166.

[32] I. Abuetwirat, K. Liedermann, Dielectric properties of thin tantalum oxide layers at solid tantalum capacitors, in: Proceedings of the International Conference on Computer Information Systems and Industrial Applications, Atlantis Press, 2015/06, pp. 889–891.

[33] Y. Guo, M. Bo, Y. Wang, Y. Liu, C. Q. Sun, Y. Huang, Tantalum surface oxidation: bond relaxation, energy entrapment, and electron polarization, Applied Surface Science 396 (2017) 177–184.

[34] P. E. Blöchl, Projector Augmented-Wave method, Phys. Rev. B 50 (1994) 17953–17979.

[35] Y. Zhang, W. Yang, Comment on "generalized gradient approximation made simple", Phys. Rev. Lett. 80 (1998) 890–890.

[36] J. P. Perdew, K. Burke, M. Ernzerhof, Generalized gradient approximation made simple, Phys. Rev. Lett. 77 (1996) 3865–3868.

[37] W. Li, H. Li, J. Li, X. Cheng, Z. Zhang, F. Chai, H. Zhang, T. Yang, P. Duan, D. Lu, Y. Chen, TOF-SIMS surface analysis of chemical components of size-fractioned urban aerosols in a typical heavy air pollution event in beijing, J. Environ. Sci. (China) 69 (2018) 61–76.

[38] P. Clabaut, R. Staub, J. Galiana, E. Antonetti, S. N. Steinmann, Water adlayers on noble metal surfaces: Insights from energy decomposition analysis, J. Chem. Phys. 153 (2020) 054703.

[39] R. Ludwig, How does water bind to metal surfaces: Hydrogen atoms up or hydrogen atoms down?, Angew. Chem. Int. Ed. 42 (2003) 3458–3460.

[40] M. J. Frisch, G. W. Trucks, H. B. Schlegel, G. E. Scuseria, M. A. Robb, J. R. Cheeseman, G. Scalmani, V. Barone, B. Mennucci, G. A. Petersson, H. Nakatsuji, M. Caricato, X. Li, H. P. Hratchian, A. F. Izmaylov, J. Bloino, G. Zheng, J. L. Sonnenberg, M. Hada, M. Ehara, K. Toyota, R. Fukuda, J. Hasegawa, M. Ishida, T. Nakajima, Y. Honda, O. Kitao, H. Nakai, T. Vreven, J. A. Montgomery, Jr., J. E. Peralta, F. Ogliaro, M. Bearpark, J. J. Heyd, E. Brothers, K. N. Kudin, V. N. Staroverov, R. Kobayashi, J. Normand, K. Raghavachari, A. Rendell, J. C. Burant, S. S. Iyengar, J. Tomasi, M. Cossi, N. Rega, J. M. Millam, M. Klene, J. E. Knox, J. B. Cross, V. Bakken, C. Adamo, J. Jaramillo, R. Gomperts, R. E. Stratmann, O. Yazyev, A. J. Austin, R. Cammi, C. Pomelli, J. W. Ochterski, R. L. Martin, K. Morokuma, V. G. Zakrzewski, G. A. Voth, P. Salvador, J. J. Dannenberg, S. Dapprich, A. D. Daniels, O. Farkas, J. B. Foresman, J. V. Ortiz, J. Cioslowski, D. J. Fox, Gaussian 09 Revision C.01, gaussian Inc. Wallingford CT 2009 (2009).

[41] B. Ruscic, Active thermochemical tables: Sequential bond dissociation enthalpies of methane, ethane, and methanol and the related thermochemistry, The Journal of Physical Chemistry A 119 (28) (2015) 7810–7837.

[42] D. B. Kinghorn, L. Adamowicz, Electron affinity of hydrogen, deuterium, and tri-

tium: A nonadiabatic variational calculation using explicitly correlated gaussian basis functions, The Journal of Chemical Physics 106 (11) (1997) 4589–4595.

[43] A. V. Phelps, Cross sections and swarm coefficients for H^+, H_2^+, H_3^+, H, H_2, and H^- in H_2 for energies from 0.1 ev to 10 keV, J. Phys. Chem. Ref. Data 19 (1990) 653–675.

[44] S. J. Araki, R. E. Wirz, Ion–neutral collision modeling using classical scattering with spin-orbit free interaction potential, IEEE Trans. Plasma Sci. 41 (2013) 470–480.

[45] A. Jablonski, C. Powell, The electron attenuation length revisited, Surf. Sci. Rep. 47 (2002) 33–91.

[46] M.-Y. Song, J.-S. Yoon, H. Cho, Y. Itikawa, G. P. Karwasz, V. Kokoouline, Y. Nakamura, J. Tennyson, Cross sections for electron collisions with methane, J. Phys. and Chem. Ref. Data 44 (2015) 023101.

[47] A. Gadoum, D. Benyoucef, Set of the electron collision cross sections for methane molecule, IEEE Trans. Plasma Sci. 47 (2019) 1505–1513.

[48] Y. Suzuki, T. Kizuka, Surface reconstruction in gold nanowires, Sci. Rep. 8 (2018) 9836.

[49] D. Stacchiola, J. B. Park, P. Liu, S. Ma, F. Yang, D. E. Starr, E. Muller, P. Sutter, J. Hrbek, Water nucleation on Gold: Existence of a unique double bilayer, J. Phys. Chem. C 113 (2009) 15102–15105.